Comparison of two-dimensional and three-dimensional models for profile simulation of poly-Si etching of finite length trenches

Robert J. Hoekstra[a] and Mark J. Kushner[b]
Department of Electrical and Computer Engineering, University of Illinois, Urbana, Illinois 61801

(Received 4 June 1998; accepted 20 July 1998)

The development of two-dimensional (2D) profile simulators for fabrication of microelectronics features has significantly progressed during the past few years and now enables modeling of etch profile evolution for many different plasma processing conditions. Increasingly complex devices which have three-dimensional (3D) (that is, asymmetric) structures are now being designed. These structures require improved dimensionality in profile simulators to capture their most important features. Under many conditions, such as circular via etching, two-dimensional profile simulators can be used to address 3D structures. A legitimate issue is to what degree these 2D approaches can indeed be applied to truly 3D structures. In this article, we present results from a 3D profile simulator for the purpose of comparing profiles for innately 3D features to results obtained from a 2D profile simulation. It has been found that profiles obtained from the 3D simulators exhibit greater sidewall sloping in three-plane corners than predicted by the 2D simulator. The implication to process design is that a greater degree of overetching will be required to clear these corners than predicted by the 2D simulators. Asymmetries as well as the angular spread of the ion flux distribution are examined to determine their role in 3D profile evolution. © *1998 American Vacuum Society.* [S0734-2101(98)01706-0]

I. INTRODUCTION

The development of two-dimensional (2D) profile simulators to investigate fabrication of microelectronics features during plasma etching has rapidly progressed during recent years.[1–3] An increasing sophistication in both the algorithms and the physical phenomena captured in these models have enabled their application to a wide range of processes. For example, 2D profile simulators have been applied to analysis of overhang structures to determine reactive sticking coefficients of radicals,[2] microtrenching,[4] ionized metal physical vapor deposition,[5] analysis of radical beam experiments,[6] and silicon dioxide deposition from tethraethylorthosilicate (TEOS):[7] A limited number of three-dimensional (3D) plasma etch profile models have also been reported.[8] As expected, 3D models using analytic methods such as string methods are more computationally intensive than 2D models due, in part, to the need to repeatedly generate view factors of incoming plasma species to points along an evolving 3D surface. This requirement is somewhat relaxed by using Monte Carlo simulators in which view angle factors are not explicitly calculated. However, the computational burden of 3D Monte Carlo models increases from $O(n^2)$ to $O(n^3)$ as compared to 2D models. As a result, using either method one is motivated to use 2D models whenever possible and apply or extrapolate the results to 3D structures.

Clearly, 2D models are adequate for analyzing long trenches which inherently have a 2D character or for analyzing 3D features which have advantageous symmetry, such as circular vias. However, a quantitative assessment of the appropriateness of extrapolating profiles obtained with 2D simulators to represent 3D features of finite length has not been made in any general fashion. This assessment is particularly important with regard to the use of profile models to analyze the fabrication of finite length 3D features as may be used in, for example, shallow isolation trenches. In this article, we discuss results from a study in which a newly developed 3D Monte Carlo (MC) based profile simulator has been used to investigate etch profiles for short trenches produced in poly-Si. These results are compared to profiles obtained with a 2D simulator using identical algorithms to determine under what conditions the 3D representation is required. The study is performed using an integrated model which combines a comprehensive plasma equipment simulator with the MC feature profile model. The purpose of this study is to both investigate the properties of etching 3D features and to make an assessment of when results from 2D simulators can be extrapolated to 3D features. Both the angular asymmetry and the angular spread of the ion flux are examined to determine their effect on profile evolution and the 3D nature of the feature. The role of redeposited etch products is also examined for these conditions.

The model will be described in Sec. II. Profiles predicted by the 3D simulator for asymmetric and symmetric ion flux distributions are discussed in Secs. III and IV. Our concluding remarks are in Sec. V.

II. DESCRIPTION OF THE PROFILE MODEL

The modeling hierarchy employed in this study has been previously described[9] and so will be only briefly discussed here. The integrated plasma equipment-feature profile model consists of three major components: the hybrid plasma equipment model (HPEM),[10] the plasma chemistry Monte Carlo simulation (PCMCS),[11] and the Monte Carlo feature

[a]Electronic mail: stretch@uigela.ece.uiuc.edu
[b]Author to whom correspondence should be addressed; electronic mail: mjk@uiuc.edu

profile model (MC-FPM).[9] The HPEM is a 2D modular simulation which combines an electromagnetic module, an electron kinetics module, and a fluid model in an iterative fashion. The HPEM produces electric fields, ion and neutral densities, and particle source distributions as a function of position, as well as the magnitude of ion and neutral fluxes incident on to the wafer. The HPEM uses a fluid model for heavy particle transport, and so particle energy distributions (PEDs) and particle angular distributions (PADs) for neutrals and ions striking the wafer are not directly available. These distributions are produced by the PCMCS.[11] The PCMCS calculates the trajectories of neutral and ion plasma species in the gas phase and their collisions with surfaces. It uses sources of plasma species, time dependent electric fields, and time dependent sheath properties generated by the HPEM. The PCMCS then produces PEDs and PADs of all plasma species intersecting with all surfaces, including the wafer. The MC-FPM then uses these PADs and PEDs as a function of position on the wafer to generate etch profiles.

The MC-FPM uses Monte Carlo methods to both follow the trajectories of reactive species and products, and to evolve an etch profile based on the fluxes, PADs, and PEDs generated by the PCMCS. The 2D version of the MC-FPM is described in Ref. 9. The 3D version applied to this study is essentially identical to the 2D model with respect to algorithms and methodology with the exception of the added dimensionality. The Monte Carlo method, as opposed to semianalytic methods, was chosen due to the ease of implementing surface reaction mechanisms of user defined complexity and which are energy dependent. The MC method also eliminates the need for computing view factors of incoming species since the trajectories of reactants and products, the flux to a point on the surface, and the advance of the surface are statistically determined.

The MC-FPM resolves the trench region on the wafer (mask and semiconductor) in 2D or 3D using a rectilinear mesh. The mesh spacing is typically 200–500 cells for a 1 μm length. Each computational cell is therefore as small as 10 atoms on a side. Each cell is assigned a material identity (e.g., poly-Si, photoresist, SiO_2, plasma) which may change during the simulation. Gas phase species (i.e., radicals and ions) are represented by computational pseudoparticles. Solid species, including adsorbates or passivation, are represented by the identity of the computational cell. The MC-FPM begins by launching pseudoparticles representing radicals and ions towards the surface with initial trajectories (energy and angle) randomly chosen from the PEDs and PADs provided by the PCMCS. The pseudoparticles are launched with a frequency computed from the total flux of radicals or ions incident onto the substrate so that each pseudoparticle represents approximately the number of solid atoms in a single computational cell. The effects of surface charging on the profile evolution, an option in the model, are not addressed here since we are primarily interested in the etching of fairly conductive materials.

A generalized reaction scheme for interaction of the ions and neutrals with the surface is used in the MC-FPM which allows for any reactant–product combination, and allows for an energy dependence of the interaction. The classes of reactions in the model include adsorption, passivation, ion activated etching, thermal etching, sputtering, ion or neutral reflection, and re-emission. In this work, we are examining etching of Si using chlorine plasmas. The mechanism we have adopted is based on the works of Cheng *et al.*[12] and Meeks and Shou,[13] and is discussed in detail in Ref. 9. Etching takes place by first successively chlorinating the polysilicon surface, forming $SiCl_n$ (i.e., SiCl followed by $SiCl_2$, and so on). Etching of the poly-Si and evolution of the $SiCl_n$ etch product then occurs through subsequent ion bombardment. The silicon dioxide underlayer to the poly-Si is etched with an arbitrarily chosen selectivity of 1:50 relative to poly-Si.

III. PROFILES FOR FINITE LENGTH STRUCTURES WITH ANGULARLY ASYMMETRIC ION FLUXES

The test feature for this study is an 0.8 μm long by 0.4 μm wide trench having a 0.3 μm thick hard mask. The plasma tool is an inductively coupled plasma (ICP) reactor operating at 10 mTorr of Cl_2, 800 W of inductively coupled power with a 150 V bias (13.56 MHz) on the substrate. The total positive ion flux to the wafer, composed of Cl_2^+ and

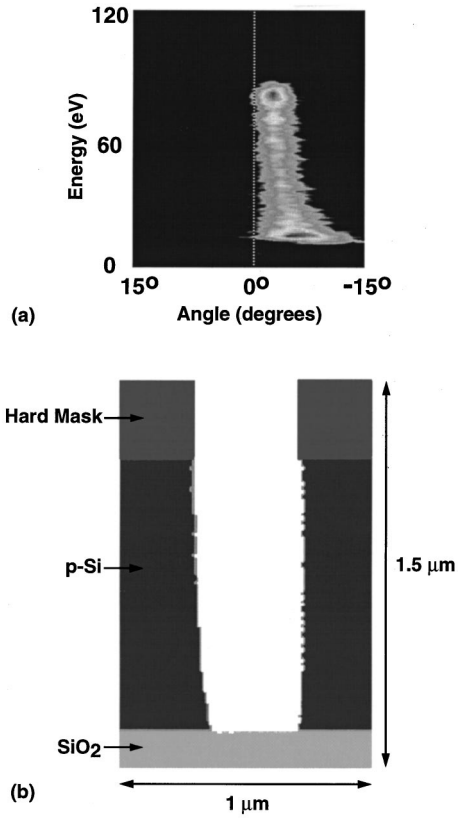

FIG. 1. (a) Asymmetric ion energy and angular distribution for an ICP reactor obtained with the HPEM and PCMCS. The operating conditions are 10 mTorr, 100 sccm Cl_2, 800 W ICP, and 150 V chuck bias at 13.56 MHz. (b) Etch profile obtained with the 2D simulator for an infinitely long trench in polysilicon. The mask opening is 0.4 μm. The shading on the walls of the trench indicates chlorinated surfaces (e.g., $SiCl_n$) or passivation.

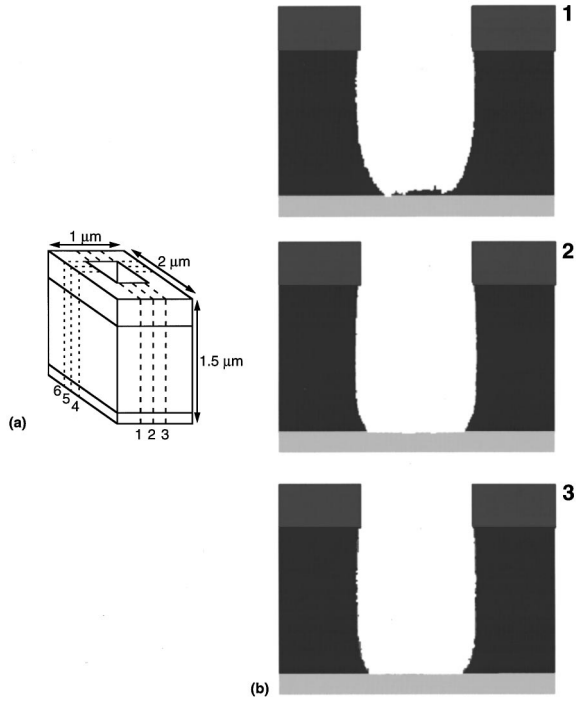

FIG. 2. Etch profiles obtained with the 3D model for a 0.4 μm$\times$0.8 μm long trench. (a) Schematic showing the locations of axial profiles perpendicular to the short axis (profiles 1, 2, and 3) and transverse profiles perpendicular to the long axis (profiles 4, 5, and 6). (b) Axial profiles parallel to the long axis of the trench at locations 1, 2, and 3. The asymmetry in the profile worsens and the etch rate decreases when one approaches the endwall. The shading on the walls of the trench indicates chlorinated surfaces (e.g., $SiCl_n$) or passivation.

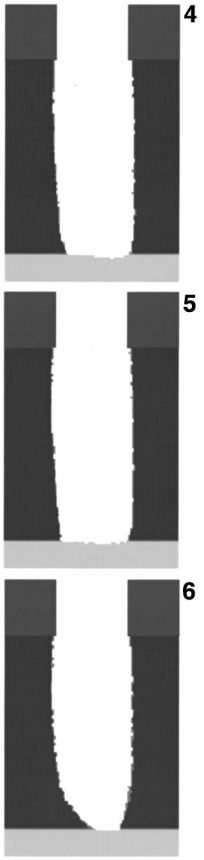

FIG. 3. Transverse etch profiles obtained with the 3D model in planes perpendicular to the long axis of a 0.4 μm$\times$0.8 μm long trench at locations 4, 5, and 6 as indicated in the schematic in Fig. 2(a).

Cl^+, is 4.2×10^{15} cm^{-2} s^{-1}, while the Cl atom flux is 3.1×10^{18} cm^{-2} s^{-1}. The first etch profiles will be examined using the perturbed ion energy and angular distribution (IEAD) shown in Fig. 1(a). The IEAD has an angular spread of $\pm3°$ and an asymmetry of $\sim3°$ produced by an electrically interfering subwafer structure.[9] This asymmetric IEAD was purposely chosen so that significant overetching would be required to clear the feature, and so the effects being discussed here would be emphasized. The angular asymmetry shown in Fig. 1(a) is in the plane perpendicular to the long axis of the trench. The angular distribution in the direction of the long axis is symmetric with a spread of $\pm3°$. Etch profiles obtained with symmetrically broadened IEADs will be discussed in Sec. IV.

The etch profile obtained with the 2D model for the asymmetric IEAD is shown in Fig. 1(b) for 150 s of etch time. The average etch rate to the time at which the first point on the bottom of the trench is cleared is 4000 Å min^{-1}. At this time, the profile has generally smooth walls with a small slant, approximately 6°, due to the asymmetry in the ion flux. As a result of this asymmetry, the entire bottom of the trench is not simultaneously cleared. An overetch of 15% is required to completely clear the bottom of the trench.

Two-dimensional ''slices'' through the structure in planes parallel to the long axis of the trench as predicted by the 3D model are shown in Fig. 2. The locations of these 2D slices (profiles 1, 2, and 3) are indicated by the schematic in Fig. 2(a). Two-dimensional transverse slices through the structure in planes perpendicular to the long axis of the trench (profiles 4, 5, and 6) are shown in Fig. 3. The etch profile perpendicular to the long axis at the center of the trench (profile 4, Fig. 3) is similar to that predicted by the 2D model. There is, however, somewhat greater bowing of the sidewalls in the profile from the 3D model indicating an increased sensitivity to the asymmetric IEAD. This result suggests that at this location (0.4 μm from the ends of the trench) there are few 3D perturbations produced by the finite length of the trench and, to first order, the 2D model can produce acceptable profiles. Although the profiles are similar, 175 s was required to fully clear the floor of the trench to the oxide underlayer using the 3D model while only 150 s was required using the 2D model. The longer etch time predicted by the 3D model is caused by lower fluxes of reactants due to shadowing by the ends of the trench, particularly of the isotropic neutral radicals which produces a somewhat lower chlorination of the surface.

The effect of the angular asymmetry of the IEAD can be more clearly seen in the etch profiles parallel to the long axis of the trench as shown in Fig. 2(b). Near the ''shadowed'' side of the trench (profile 1), the profile has not fully cleared, and there is significant curvature at the base of the endwalls.

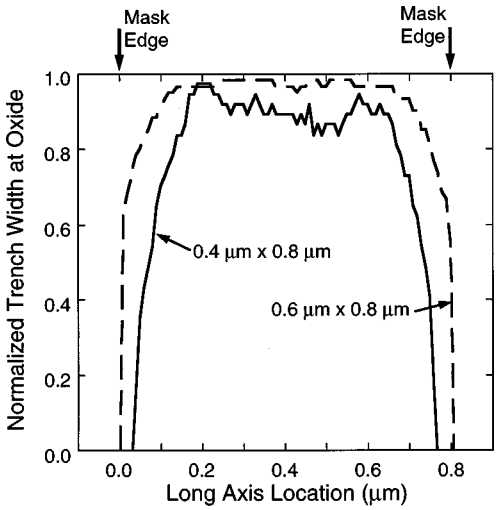

FIG. 4. Relative trench width as a function of axial location for 0.4 μm $\times$0.8 μm and 0.6 μm$\times$0.8 μm trenches. The relative trench width is the width of the exposed oxide on the floor of the trench divided by the width of the mask opening. The narrower trench has lower etch rates near the endwalls due to the proximity of the three-plane corners.

Near the ''unshadowed'' side of the trench (profile 3), the trench has fully cleared and etching of the oxide has begun. The curvatures of the profiles at the base of the endwalls for the longitudinal profiles are noticeably larger than the curvature at the base of the transverse trench sidewalls. This disparity is due to the 3D shadowing of reactants which is most severe near the ends of the trench near the three-plane corners.

The transverse etch profile near the edge of the trench (profile 6, Fig. 3) is dramatically underetched, even after a 30% overetch relative to the center of the trench (profile 4) which is fully cleared. There is also a larger side-to-side overetch requirement due to the asymmetry in the IEAD. This asymmetry produces a lower etch rate on the side of the trench which is more severely shadowed. Within a tenth of a micron from the endwall, the profiles predicted by the 3D model significantly deviate from those predicted by the 2D model. Shadowing of the IEAD in the three-plane corners which reduces the ion and radical fluxes is largely responsible. Proximity to the 3D corners is therefore a measure of the appropriateness of the 2D model.

The importance of the proximity to the three-plane corners for assessing the validity of 2D simulators is shown in Fig. 4. The normalized widths of the trench at the oxide layer after 175 s of etching are plotted for 0.4 μm$\times$0.8 μm and 0.6 μm$\times$0.8 μm features. (The normalized width is the exposed width of the oxide at the bottom of the trench divided by the width of the mask opening.) The proximity of the three-plane corners is commensurably higher for the 0.4 μm wide trench than for the 0.6 μm wide trench. The narrower aspect ratio trench has both a smaller etch rate and clears the trench bottom for smaller a fraction of its length along the long axis. It is also more sensitive to the side-to-side asymmetry in the IEAD.

An extreme case of proximity of 3D plane corners is a square via. For example, profiles of a square 0.4 μm via etched for 175 s produced by the 3D model are shown in Fig. 5. These profiles clearly exhibit the consequences of three-plane corner shadowing. There is significant tapering of the feature produced by the nearness of 3D plane corners. The asymmetry of the IEAD produces an asymmetry in the profile which is magnified by the proximity of the three-plane corners compared to the longer aspect ratio trenches. These effects result in requiring longer overetch etch times (>30%) than would be predicted by the 2D model. The horizontal plane views shown in Fig. 5(b) demonstrate the increasing consequences of the finite 3D nature of the feature resulting from the asymmetry of the IEAD as the feature increases in depth.

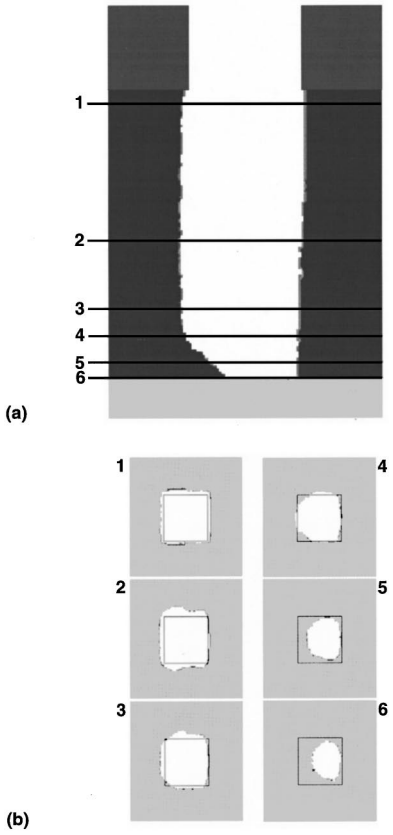

FIG. 5. Etch profiles for a square 0.4 μm$\times$0.4 μm via. (a) Transverse etch profile in the plane of the asymmetry in the IEAD. (b) Horizontal slices at the heights (labeled 1–6) noted in (a). These results show the increasing effects of the finite 3D nature of the feature and of the asymmetric IEAD as etch depth increases.

IV. PROFILES FOR FINITE LENGTH STRUCTURES WITH ANGULARLY SYMMETRIC ION FLUXES

In Sec. III, an IEAD having a $\pm$3° angular spread and an off axis asymmetry was used to demonstrate 3D effects on the etch profiles of finite length trenches. To systematically examine the consequences of the angular distribution on the evolution of these finite length trenches, an angularly symmetric IEAD from an unperturbed location on the substrate was used as a base distribution. The IEAD, in addition to having a symmetric angular distribution, has a slightly higher maximum energy of 100 eV but still retains the $\pm$3° angular

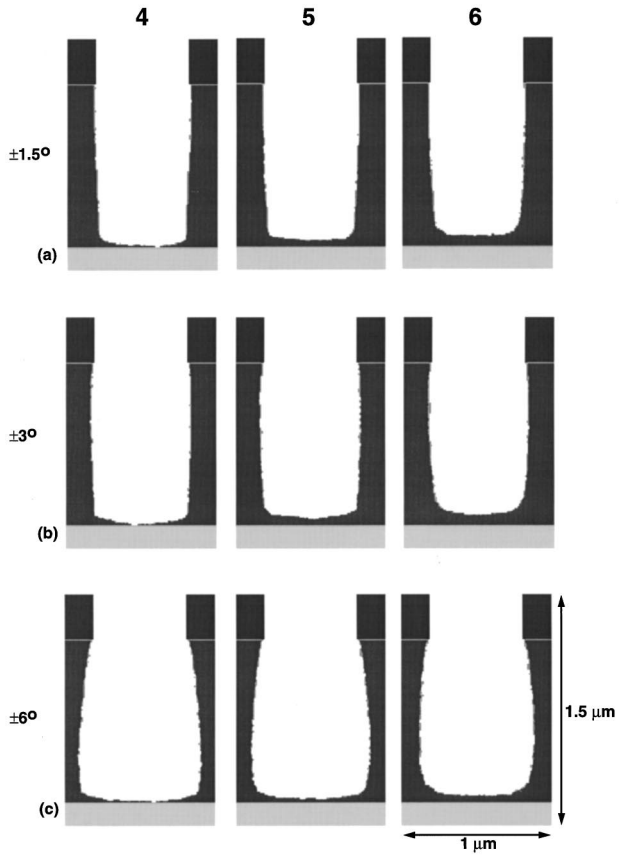

FIG. 6. 2D profiles perpendicular to the long axis of a 0.6 μm×0.8 μm trench at locations 4, 5, and 6 as noted in Fig. 2(a) for a sticking coefficient of 0.10 for redeposited $SiCl_n$. The angular spreads of the IEADs are (a) ±1.5°, (b) ±3°, and (c) ±6°. The shading on the walls of the trench indicates chlorinated surfaces (e.g., $SiCl_n$) or passivation.

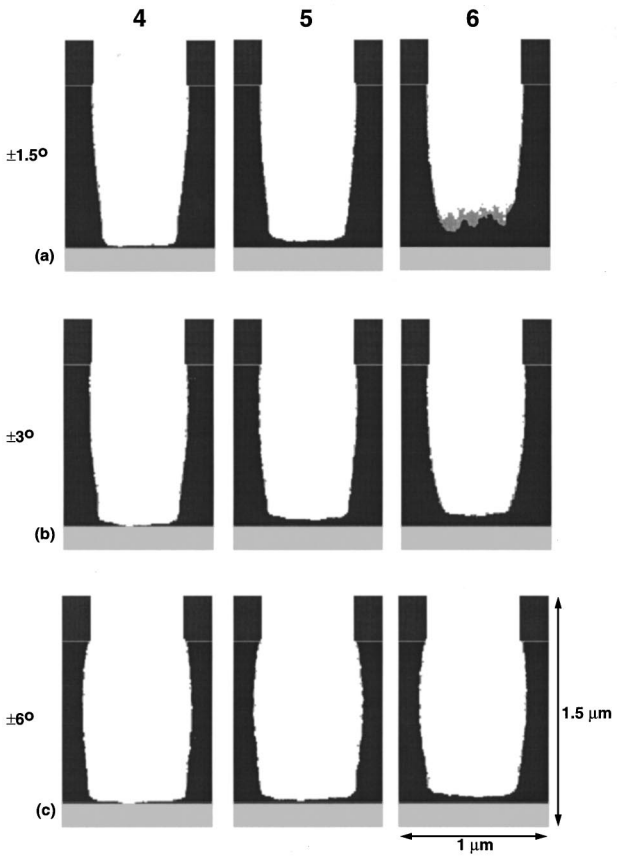

FIG. 7. 2D profiles perpendicular to the long axis of a 0.6 μm×0.8 μm trench at locations 4, 5, and 6 as noted in Fig. 2(a) for a sticking coefficient of 0.30 for redeposited $SiCl_n$. The angular spreads of the IEADs are (a) ±1.5°, (b) ±3°, and (c) ±6°. For the narrow IEAD, sidewall tapering leads to a decrease in the etch rate as large as 20% near the ends of the feature. The shading on the walls of the trench indicates chlorinated surfaces (e.g., $SiCl_n$) or passivation.

spread. The effects of a narrowing or broadening the angular spread of the IEAD on the 3D etch profile were examined by adjusting this IEAD to have an angular spread of ±1.5° and ±6°. These three IEADs were then used with the MC-FPM to simulate the etching of a 0.6 μm×0.8 μm feature. Results will be discussed for two values of the sticking probability for redeposition of the $SiCl_n$ etch product, 0.1 and 0.3.[14]

Etch profiles perpendicular to the long axis of the trench [locations 4, 5, and 6 of Fig. 2(a)] are shown in Fig. 6 for the ±1.5°, ±3°, and ±6° IEADs. The sticking coefficient for $SiCl_n$ is 0.1. Etching was performed until initial contact with the oxide layer. The intuitive results are that as the IEAD becomes more narrow, the sidewall slope should become more shallow, and the three-plane corners should become less rounded. In the extreme case of an IEAD with zero angular spread and for an ion activated etch process, one would expect little, if any, variation in the transverse etch profile along the axis of a finite length trench. To some degree, this intuition is confirmed by the results in Fig. 6. For the narrow IEAD (±1.5°), the profiles are fairly uniform along the trench with a slight inward slope. The etch rate is smaller near the wall due to shadowing of the reactive fluxes, with some additional rounding in the three-plane corners. As the IEAD broadens, the differences in transverse profiles between the center and edge of the trenches become more pronounced. In the most severely broadened case (±6°), the profile is significantly undercut in the center of the trench. However, as the endwall is approached, the undercutting lessens and the etch rate decreases. In this case, shadowing in the three-plane corners of reactants having large angular spread is beneficial by intercepting large angle ions which lead to undercutting.

Etch profiles perpendicular to the long axis of the trench [locations 4, 5, and 6 of Fig. 2(a)] are shown in Fig. 7 for the ±1.5°, ±3°, and ±6° IEADs when the sticking coefficient for the $SiCl_n$ etch product is 0.3. Etch profiles in the center of the trench aligned with the long axis for this case are shown in Fig. 8. For the ±1.5° IEAD, there is a large variation in the transverse profiles shape and etch rate between the center of the feature and locations near the end of the trench. In particular, the sidewalls have a significant inward slope which worsens near the endwalls. As the IEAD broadens to ±3°, the walls straighten and the etch rate becomes more uniform. For the ±6° IEAD, the distribution is sufficiently broad that undercutting has started; however the profiles are fairly uniform along the length of the trench.

These results are somewhat counterintuitive, in that a

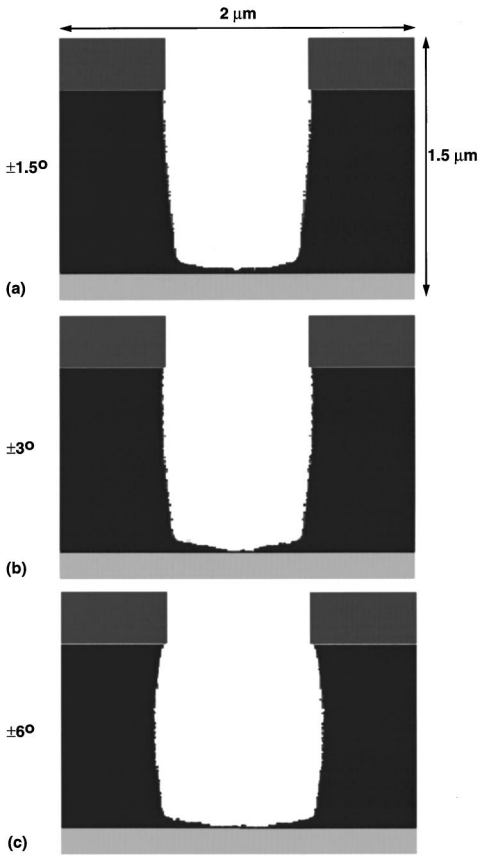

FIG. 8. 2D profiles parallel to the long axis of the trench and centered along the short axis of the feature [profile 1 in Fig. 2(a)] for a sticking coefficient of 0.30 for redeposited $SiCl_n$. The angular spreads of the IEADs are (a) $\pm 1.5°$, (b) $\pm 3°$, and (c) $\pm 6°$.

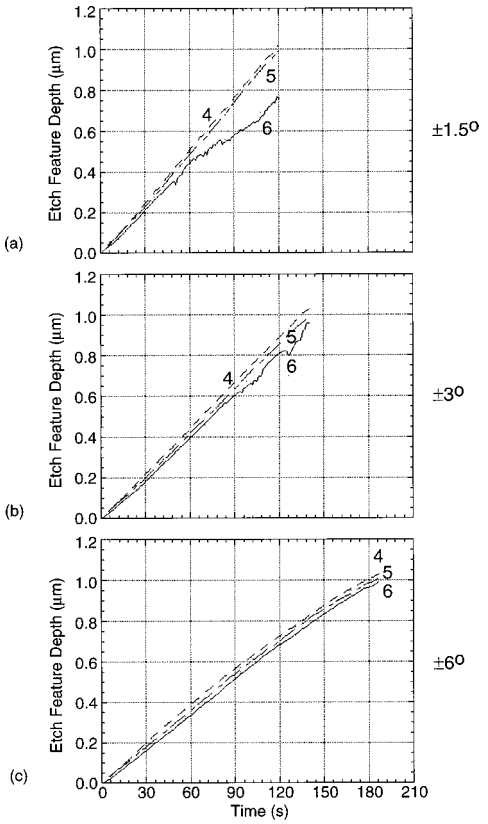

FIG. 9. Time evolution of the trench depth at the three transverse locations (profiles 4, 5, and 6) for the conditions of Figs. 7 and 8. The angular spreads of the IEADs are (a) $\pm 1.5°$, (b) $\pm 3°$, and (c) $\pm 6°$. Locations far from the endwalls (profiles 4 and 5) show nearly linear etch rates with time. Locations near the wall (profile 6) have a lower etch rate. The overall etch rate can also be seen to be inversely dependent on the angular spread of the incoming IEAD. Aspect ratio dependent etch becomes more significant as the angular spread increases.

broader IEAD actually results in a more uniform, more anisotropic etch profile along the trench one which is less sensitive to three-plane corners. This trend is a consequence of the redeposition of etch products on the sidewalls. The $SiCl_n$ etch products are isotropically and diffusively emitted from the etched surface. The etch products reflect off the side- and endwalls in leaving the trench. Some of the $SiCl_n$ redeposits on the sidewalls, endwalls, and in the corners. These etch products are, to some degree, passivation which slows the etch and must be removed from the surface by ions for etching to continue. This cleansing requires some breadth to the IEAD. The sidewall (endwall) slope can be attributed to this passivation since the flux of the passivation to the walls is higher at the bottom of the trench. The effect is more severe in the three-plane corners due to there being more shadowing of the IEAD, thereby allowing more passivation to accumulate on the sidewalls (endwalls).

The demonstrated sensitivity of etch profiles in 3D structures to the breadth of the IEAD and the redeposition of etch products may lend some insight into requirements for scaling processes developed for 2D structures to 3D structures. For example, sticking coefficients on sidewalls (endwalls) for etch products are sensitive functions of temperature. Small excursions in wafer temperature which change these coefficients may result in only small changes in 2D etch profiles (or in profiles far from three-plane corners). The same variation in sticking coefficients may produce significant changes in etch profiles and etch rates near three-plane corners. This trend results in overetch times being a function of wafer temperature. Similarly, the bias voltage is often varied during a process which, in turn, produces small variations in the angular spread of the IEAD. These variations in IEAD do not significantly change 2D etch profiles but may produce significant changes in profiles and etch rates near three-plane corners.

Etch depths as a function of time for different angular spreads in the IEAD and position in the trench are shown in Fig. 9 for the case where the sticking coefficient for $SiCl_n$ is 0.3. Etch depths are shown for transverse etch profiles at locations 4, 5, and 6 [see Fig. 2(a)]. As the angular distribution is broadened, the etch rate decreases. For example, the $\pm 6°$ IEAD feature requires $\approx$190 s to reach the depth of the oxide while the $\pm 1.5°$ IEAD feature only requires only $\approx$120 s. This dependence of etch rate on breadth of the IEAD is due to the greater shadowing of the $\pm 6°$ IEAD as the trench depth increases. Note also that the narrow IEADs have, at least in the middle of the feature, nearly linear etch rates while the broad IEADs have a significant aspect ratio dependent etch rate (i.e., an etch rate that decreases with

depth). The variation in the etch rate along the trench varies inversely with the breadth of the distribution due to the cited need to remove passivation from the sidewalls (endwalls). The $\pm 1.5°$ IEAD has a 20% variation in etch rate between the middle of the trench and near the endwall, whereas the $\pm 6°$ feature has only a 5% variation. For these conditions, the $\pm 3°$ IEAD maintains the best balance between overall feature conformity and etch rate, requiring 140 s to reach the oxide with a minimum amount of overetch required.

V. CONCLUDING REMARKS

We have compared predictions for etch profiles for finite length trenches obtained from 2D and 3D Monte Carlo simulators for particularly harsh conditions produced by both aspect ratio and asymmetry of the IEAD. For the feature with an aspect ratio of 1:2:2.5 (0.4 μm wide, 0.8 μm long, and 1.0 μm deep), the 2D model produces transverse profiles very similar to the 3D model at the center of the long axis, although the 2D model overpredicts the etch rate by approximately 20% due to the lack of large angle shadowing by the endwalls. The transverse profiles from the 3D model within a tenth of a micron from the endwall differ significantly from that of the 2D model. There is more rounding of the corners produced by shading at the three-plane corners and reduced etch rates, thereby requiring longer overetch times than would be predicted by the 2D model. This is particularly evident in profiles parallel to the long axis. As the aspect ratio of the mask opening increases to that of a square via, the shadowing at the three-plane corners overlaps, producing a tapered feature with a rounded bottom. Profiles obtained from 2D models for these structures should be scrutinized.

The role of the angular spread of the IEAD in the presence of redeposition of etch products was also examined. It was found that for narrow angular distributions (spreads $<3°$) with large probabilities for redeposition, the inward taper of the sidewalls at the ends of the trench produced a strong differential in etch rate between the ends and the center of the feature. For broader distributions, the sidewalls do not encroach on the feature and a more uniform etch rate is maintained across the bottom of the feature. This result was dependent on the rate of redeposition of $SiCl_n$. As this sticking coefficient was lowered, the angular spread could be reduced without inducing the inward taper of sidewalls and endwalls. These results indicate that the sidewall slope and corner curvature as well as the differential etch rate over the feature bottom are dependent on the three-dimensional aspect ratio of the feature as well as on the angular spread of the IEAD and the redeposition rate of etch species.

ACKNOWLEDGMENTS

The authors thank Dr. Chris Foster for his comments on the implication of these results. This work was supported by the Semiconductor Research Corporation, the National Science Foundation (Grant Nos. ECS 94-04133 and CTS 94-12565), and the University of Wisconsin ERC for Plasma Aided Manufacturing.

[1]S. Hamaguchi and M. Dalvie, J. Vac. Sci. Technol. A **12**, 2745 (1994).
[2]V. K. Singh, E. S. G. Shaqfeh, and J. P. McVittie, J. Vac. Sci. Technol. B **12**, 2952 (1994).
[3]B. Abraham-Strauner and W. Chen, J. Vac. Sci. Technol. B **14**, 3492 (1997).
[4]T. J. Dalton, J. C. Arnold, H. H. Sawin, S. Swan, and D. Corliss, J. Electrochem. Soc. **140**, 2395 (1993).
[5]S. Hamaguchi and S. M. Rossnagel, J. Vac. Sci. Technol. B **13**, 183 (1995).
[6]J. P. Chang and H. H. Sawin, J. Vac. Sci. Technol. A **15**, 610 (1997).
[7]M. Virmani, D. A. Levedakis, G. B. Raupp, and T. S. Cale, J. Vac. Sci. Technol. A **14**, 977 (1996).
[8]Z. K. Hsiau, E. C. Kan, J. P. McVittie, and R. W. Dutton, IEEE Trans. Electron Devices **44**, 1375 (1997).
[9]R. J. Hoekstra, M. J. Grapperhaus, and M. J. Kushner, J. Vac. Sci. Technol. A **15**, 1913 (1997).
[10]M. J. Grapperhaus and M. J. Kushner, J. Appl. Phys. **81**, 569 (1997).
[11]R. J. Hoekstra and M. J. Kushner, J. Appl. Phys. **79**, 2275 (1996).
[12]C. C. Cheng, K. V. Guinn, V. M. Donnelly, and I. P. Herman, J. Vac. Sci. Technol. A **12**, 2630 (1994).
[13]E. Meeks and J. W. Shon (private communication).
[14]J. P. Chang, A. P. Mahorowala, and H. H. Sawin, J. Vac. Sci. Technol. A **16**, 217 (1998).